EQA - International Journal of Environmental Quality
ISSN 2281-4485 - Vol. 60 (2024): 1-17
Journal homepage: https://eqa.unibo.it/

published by

Optmisation of cadmium (II) removal onto biodegradable composite using artificial neural networks and response surface methodology: quantum chemical performance.

Jean Claude Banza*, Maurice Stephane Onyango

Department of Chemical, Metallurgical and Materials Engineering, Tshwane University of Technology, Pretoria, South Africa

* Corresponding author E-mail: banzamjc@tut.ac.za

Article info
Received 6/12/2023; received in revised form 21/12/2023x; accepted 3/1/2024
DOI: 10.6092/issn.2281-4485/18602

Abstract

A multifunctional grafted cellulose nanocrystals derivative adsorbent (composites) with carboxyl, amide, and secondary amino groups was successfully developed for Cd^{2+} removal. The characteristics of CNCs, chitosan, and nanocomposites were determined using FTIR, TGA, SEM, and BET. The approaches of artificial intelligence and Response Surface Methodology modeling were employed, as well as how well they predicted response (adsorption capacity). The adsorption isotherm and kinetic models were applied to comprehend the process further. Statistical results demonstrated that The response surface model approach performed better than the artificial neural network model approach. The adsorption capacity was 440.01 mg/g with a starting pH of 5.65, a duration of contact of 315 minutes, a starting concentration of 333 mg/L, and an adsorbent dose of 16.93 mg. The FTIR examination revealed that the functional groups of the nanocomposites were equivalent to those of CNCs and chitosan; however, the nanocomposites were more thermally stable than CNCs and chitosan. The nanocomposites' SEM pictures revealed a porous structure, thin particle size, and needle-like shape. The Langmuir model explains the spontaneous nature of the adsorption process, and chemisorption served as the primary control. According to the Dubinin-Radushkevich Model, to adsorb $Cd^{2+,}$ the energy required is larger than 8 kJ mol-1, suggesting that the chemisorption mechanism was involved. The adsorption kinetics were established using the pseudo-second-order rate model. $H_{OMO}-L_{UMO}$ energy binding differences were used to find the best locations for adsorption.

Keywords

Cellulose nanocrystals, Chitosan, Quantum chemical simulation, Central composite design, Artificial neural network, Response surface method

Introduction

One of the world's most hazardous nonbiodegradable elements is metals, which are utilized in various fields: mining, electroplating, chemical, leather tanning, galvanizing, pigment, and dye industries. It is a concern due to their untreated effluents with a considerable amount of toxic metal ions discharged into the environment, posing environmental problems. Moreover, according to the United States Environmental Protection Agency (USEPA), several metals have been designated carcinogenic and bioaccumulative elements (Khadhri *et al.*, 2019; Oyewo *et al.*, 2019). The vast majority of the heavy metals that easily accumulate in aquatic animals (fish, squid, otters, oysters, swordfish etc.) and plants, are not biodegradable, eventually entering the food chain and the human body. If the accumulation of the heavy metal content in the body surpasses the micro-

DOI: 10.6092/issn.2281-4485/18602

nutrient levels, the enzyme's ability to operate will be affected; this can result in various ailments and even life-threatening disorders (Chen *et al.*, 2019). Precipitation, membrane filtration, ion exchange, adsorption, chemical reduction/oxidation, and other methods have all been employed to minimize the negative environmental effects associated with heavy metal accumulation to a suitable level (Rahaman *et al.*, 2021; Salcedo *et al.*, 2016). Selectivity, saturation, temperature, pres-sure, expense, fouling, and specificity are among the drawbacks of the adsorption process. High tempera-tures and pressures can reduce the efficiency of a selective and particular process like adsorption. Adsorbents are also susceptible to saturation and fouling, which lowers efficiency and raises costs (Punia Bangar *et al.*, 2022). The procedure's efficiency also depends on the molecules that will be adsorbed and the chemical composition of the adsorbent. As a result, many researchers are focusing on bioresource adsorbent development. Cellulose is a bioresource that has spiked the curiosity of several scholars due to its high stability, renewability, and biodegradability (Henschen *et al.*, 2019). High levels of polymerization are present in cellulose, composed of b-D-glucopyranose units joined by b1,4 glycosidic bonds. The clusters of hydroxyl groups that are present in cellulose form a highly crystallized framework due to intramolecular solid and intermolecular hydrogen interactions, which hinder its capacity to absorb heavy metal ions. In contrast, cellulose has a large number of hydroxyl groups that enable chemical modification, leading to exceptional adsorption performance and widespread application (Shahnaz *et al.*, 2020). Furthermore, prior studies have demonstrated that among bio-based natural polymer nanocomposites, composites derived from CNCs are viable biosorbents for water purification because they possess a strong affinity for various pollutants present in wastewater (Moharrami & Motamedi, 2020; Vincent & Kandasubramanian, 2021). An important advantage of gelatin's chemical structure is the presence of hydroxyl and amino groups, making it easier to functionalize and modify it with nanomaterials. Inorganic nanoparticles such as ZnO, TiO_2, Fe_3O_4, etc., and nanomaterials such as carbon nanotubes are suited to enhancing the mechanical properties of cellulose nanocrystals, which are crucial for water treatment. Furthermore, cellulose nanocrystals that have been functionnalized by adding additional functional groups to them through nanoparticles are envisaged to enhance CNCs interacting features, increase the density of adsorption sites, alter the pH level suitable for pollutants adsorption, and improve adsorption selectivity for various pollutants in water (Voisin *et al.*, 2017). A high adsorption capacity can only be attained using nanomaterials with immense surface areas and several other superb multifunctional features, such as inorganic and carbon nanoparticles. Resulting from enhanced contacts between the active sites of cellulose-based nanocomposites and the adsorbate (pollutants) (Olad *et al.*, 2020). The mechanism behind the adsorption processes is intricate. It is because of the complex interactions between many components and the non-linear character of these processes. Finding the ideal experimental settings is crucial for obtaining optimum effectiveness. Single-variable optimization is a time-consuming and ineffective technique for optimization (Nordin *et al.*, 2021). However, it ignores coupled interactions between physicochemical elements and fails to portray the complete influence of process parameters. This method may cause findings to be interpreted incorrectly. This problem has been attempted to be solved using certain statistical methods; however, recent years have seen a surge in interest in response surface methodology (RSM), a collection of mathematical and statistical methods for assessing the implications of several independent inputs (Shahnaz *et al.*, 2020). RSM examines the relationships between the response(s) and independent variables and how the independent variables, either separately or together, affect the processes. This method has several advantages, including saving time, requiring fewer trials, looking at how different elements interact to determine response, forecasting responses, and deciding whether the method is acceptable (Olatunji *et al.*, 2022). An experimental strategy frequently employed in response surface methods to ascertain the connection between independent variables (factors) and their impact on an interest response is referred to as the central composite design (CCD). Factorial and axial points joined by center points are used in CCDs. While the center points estimate pure error, the axial points enable the measurement of response surface curvature. The main advantage is that it just needs a few setting for experiments that may be established after only a few experiments (Deshwal *et al.*, 2020). The goals of the investigation and the characteristics of the investigated parameters will determine whether to use a rotatable or face-centered CCD. When the response surface is anticipated to be symmetrical around the center point, a rotatable CCD is employed. In contrast, a face-centered CCD is employed when the response surface is

DOI: 10.6092/issn.2281-4485/18602

anticipated to have a linear connection between the variables and the response at the center point (Ahmadi *et al.*, 2021). Various techniques for analyzing data based on physiological phenomenon have also developed over the past ten years into well-known modeling paradigms, including evolutionary computing and artificial intelligence. In fact, an ANN is a significantly connected network structure made up of several crucial processing elements that may do multiple computations at once (Cojocaru *et al.*, 2021). When the processes governing process performance are intricate, this strategy works well. Due to their consistent and apparent capacity to capture the factor with non-linear interconnections, artificial neural networks have been the subject of substantial study in recent years to solve environmental issues. It can address issues where conventional statistical methods fall short (Ayoola *et al.*, 2019). ANNs have been assessed due to their extensive usage, aptitude, and capacity for managing complicated problems. When no analytical model is available, chemical engineering employs ANNs for process modeling and simulation. In order to remove heavy metal ions from wastewater, the sensitivity analysis, modeling and generalization capabilities, and optimization efficiency of the RSM and ANN techniques were investigated (Ayoola *et al.*, 2019). The principal goal of this research work was to evaluate the sorption efficiency of cellulose composite, a biodegradable and inexpensive adsorbent for Cd^{2+} adsorption using the response surface method and artificial neural network, evaluate their effectiveness in the water purification method, and conduct a comparative study between the artificial neural network and response surface method techniques. The models' findings were then compared with the results of the experiments.

Materials and Methods

Materials and equipment

The Tshwane University of Technology provided the waste papers from which cellulose nanocrystals were extracted. Chitosan (75% acetylated) industrial quality. Urea (>99.5%), sodium hydroxide (>99%), hydrochloric acid (>99%), acetic acid (>99%), and cadmium acetate dihydrate were all purchased from Sigma-Aldrich. X-ray diffraction (XRD) was employed in both quantitative and qualitative methods. SEM was used to analyse the morphological appearance. Fourier transform infrared spectroscopy (FTIR) was used to examine the chemical components that made up the cellulose nanocrystals, chitosan, and composite. A thermal thermogravimetric analyzer (TGA) was employed to examine the thermal resistance of materials.

Method

Aqueous urea and water solution was created, then frozen. 200 mL of urea solution was vigorously swirled while 10 g of cellulose nanocrystals were added. The liquid was homogenized at 1000 rpm for 10 minutes after being homogenized at room temperature after being frozen at -25°C for 15 minutes to dissolve the cellulose nanocrystals. At ambient temperature, 20 g of chitosan and 2% acetic acid were mixed. 250 mL of urea, NaOH, and water were used to dissolve the chitosan powder. To freeze the material, it was immediately cooled to -15 °C. After properly defrosting, the frozen substance was agitated at 1500 rpm for 10 minutes. A needle-like instrument was used to inject 30 mL of cellulose nanocrystal the mixture at a rate of 5 mL per minute into 30 mL of chitosan. An electromagnetic bar was used to mix the solution at 500 rpm after injection. After collection, the composite was cautiously cleaned with deionized water to get rid of the salts before drying.

Batch experiments. In 250 mL glass flasks, batch adsorption tests were conducted using cellulose nanocrystal/chitosan nanocomposites to remove Cd^{2+}. The nanocomposites were added to 200 mL of Cd^{2+} solution, with pH from 2 to 8, the initial from 50 to 500 mg/L, and were combined with 5 to 25 mg/L of the nanocomposite. Using 1 M 1 M HCl and NaOH, the pH of the solution was adjusted while the glass beakers were covered in parafilm to protect it. After that, the collected material was placed on a thermoshaker and shaken continuously for 0 to 360 minutes at a speed of 180 rpm. A flame atomic absorption spectrophotometer was used to measure the Cd^{2+}content in residual solutions after they reached equilibrium. Equation [1] determined the quantity of cadmium ions adsorbed onto the composite (qe).

$$\text{Adsorption capacity} = C_{in} - C_{final}) \times V/M \qquad [1]$$

where M denotes the amount of the used composite (mg), V denotes the measured volume(L), and C_{in} represents the starting amount of Cd^{2+}, and C_{final} signifies the equilibrium concentration (mg/L). Each experiment was repeated three times for accuracy, and the mean results were obtained.

DOI: 10.6092/issn.2281-4485/18602

Response surface methodology. RSM's crucial areas of experimental design are that studies must be carried out conventionally between factors that must be investigated and that one variable must change conventionally when all other variables are put to a certain value. The RSM approach evaluates how various factors interact and influence the system's reaction. It uses both mathematical and statistical methods. This approach involves fewer experimental runs and may be used to develop and improve independent variables and responses (Akhtar *et al.*, 2022). RSM is most typically used when several factors influence how the system responds. The RSM, as previously said, includes three stages: experiment design, response surface modeling, and optimization. The experimental design in this research was generated using Design Expert software, version 13. Table 1 gives the input variables which are considered, ranging from 1 to 3. Therefore, in the present investigation, the following factors were considered independent variables: Dosage (Y_3), Concentration (Y_4), pH (Y_1), and Time (Y_2) are all exponents. The adsorption efficiency (qe) was chosen as a response variable. The experimental limit was established using experiment results and prior research.

Table 1 *Input variable used for the removal of Cd^{2+} (CCD)*

Parameters	Code	Level code		
pH	Y_1	2	4	8
Time	Y_2	0	120	360
Dosage	Y_3	5	12.5	25
Concentration	Y_4	50	225	500

In Equation [2], the mathematical relationship between the independent process variables is shown by the second-order polynomial.

$$X = \gamma_0 + \gamma_a Y_1 + \gamma_b Y_2 + \gamma_c Y_3 + \gamma_d Y_4 + \gamma_{aa} Y_1^2 + \gamma_{bb} Y_2^2 + \gamma_{cc} Y_3^2 + \gamma_{dd} Y_4^2 + \gamma_{ab} Y_1 Y_2 + \gamma_{ac} Y_I Y_3 + \gamma_{ad} Y_1 Y_4 + \gamma_{bc} Y_2 Y_3 + \gamma_{bd} Y_2 Y_4 + \gamma_{dc} Y_3 Y_4 \quad [2]$$

where the expected outcome (X), independent factors (Y_1, Y_2, Y_3 and Y_4), the quadratic coefficients (γaa, γbb and γcc), the model constant (γ_0 is, γ_{aa}, γ_{bb}), linear coefficients ($_{\gamma a}$, γ_b and γ), and cross-product coefficients (γab, γac and γbc).

ANN (Artificial Neural Networks). The ANN, which is well renowned for its outstanding ability to learn and categorize data, is an appropriate model for the human brain and nervous system. Artificial Neural Networks consist of both an input and an output layer, along with several hidden layers. Input values are sent to every neuron in the hidden and input layers.(Ayoola *et al.*, 2019) Neurons transmit input values to the layer of neurons below them, and weights control how strong these connections are. The best option for network training was established to be the Levenberg-Marquardt backpropagation algorithm (LMA). To predict and simulate the nanocomposite's adsorption efficiency for Cd^{2+} removal, a feed-forward three-layer ANN was also performed, combining an output layer with a linear transmission function and a hidden layer with a tangent sigmoid transmission function (Figure 1). Ten hidden layer neurons, one output node, four input nodes, and a training set with an error of 0.0001 were employed. The ANN approach was carried out using the ANN Toolbox V4.0, MATLAB, 2015a.

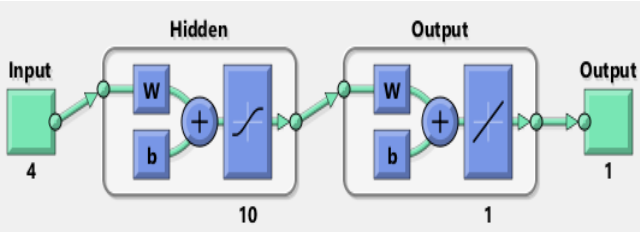

Figure 1. *Artificial neural network architecture.*

Simulation of a Quantum Mechanism. DFT was employed to examine Cd^{2+}'s ability to bind to the adsorbent. The computations for density functional theory were performed using Gaussian 6.0 software. The model cadmium form was determined to be the positively charged Cd^{2+}, while the model cellulose component was determined to be cellulose glucose. The vibrational frequency was used to demonstrate further that the molecules were appropriately optimized. The findings demonstrated no negative wavenumber peak in the spectra.(Chen *et al.*, 2019) To further understand the preferred sites for adsorption, Homo energy E.Homo, and Lumo of the adsorbent were estimated. Several chemically active

DOI: 10.6092/issn.2281-4485/18602

group-modified cellulose compounds' effectiveness was evaluated by comparing the Cd^{2+} adsorption and potential differential $E^{1/4} = E(H_{omo})-E(L_{umo})$ of various functionality of modified cellulose derivatives, the most significant number of effective adsorption regions were identified.(Mo *et al.*, 2021; Xu *et al.*, 2021) Figure 2 illustrates the nanocomposites' structure.

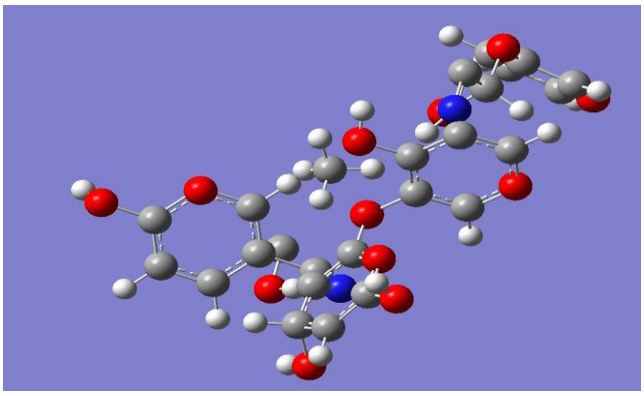

Figure 2. *The three-dimensional structure of the composite. Carbon (black), oxygen (red), nitrate (blue), and hydrogen atoms (light black).*

Results and Discussion

Figure 3a displays a peak at 3287–3485 cm^{-1} region that is linked to the vibrational stretching of the O-H. The band at 2921 cm^{-1} shows the C-H vibration linked to SP_3 hybridized carbon molecule. This band supports the hypothesis that a saturated bond encloses the carbon atom and may be seen just above 3000 cm^{-1} in the SP2 hybridized carbon area. The stretching vibration of C-O is seen at 1001 cm^{-1}. However, 790 cm^{-1}, which is recognized as the crystallinity band in any cellulosic material with glucoside linkages, reflects the overall structure of cellulose and a band at 1435 cm-1, which is representative of the CH_2 vibration (Masekela *et al.*, 2022). The normal boundaries for chitin are bands at 750, 800, 1020, 1550, 1650, 2800, 3000, and 3300 cm^{-1} (Cheng *et al.*, 2019). Figure 3b shows that the vibrations at 3320 cm-1 are linked to the N-H and O-H and stretching, while at 2990 cm^{-1} and 2799 cm^{-1} are due to the CH_3 and CH_2 vibration. Amide I at 1640 cm^{-1}, amide II, N-C, and N-H stretching vibration at 1540 cm^{-1}. The vibration of the C-O ring is at 1005 cm^{-1}. N-H had single boundaries at 790, whereas the vibration C-O occurred at 810cm^{-1}. Figure 3c shows a significant and pronounced peak between 3400 and 3600 cm^{-1} originated from the absorption bands of the hydroxyl and amine groups overlapping. The vibration of CH_2 for the composite is attributed to the band at 1499 cm^{-1}. N-H vibration caused by stretching is responsible for the evident band at 1630 cm^{-1} brought on by the overlap of carbonyl groups in CNCs and chitosan (Priya *et al.*, 2022). There is an overlap between 1150 cm-1 and 1350 cm^{-1} due to the C-O and C-N absorption bands' connection with the O-H groups' bending vibration mode. CNCs and chitosan were successfully added to the composite, as indicated by the N-H and C-O functional groups. The Cellulose nanocrystals with 50 μm magnification in Figure 4a reveal their porous nature. The homogeneous rough surface has a uniform distribution of pores, and needle-shaped fibers are visible.

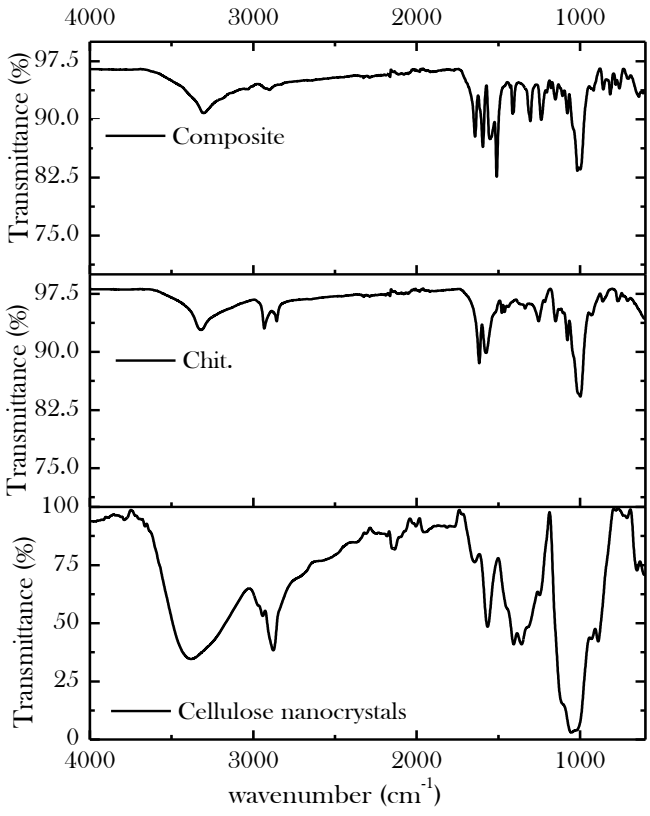

Figure 3. *Fourier transform infrared spectroscopy spectrum of composite, chitosan, and cellulose nanocrystals.*

DOI: 10.6092/issn.2281-4485/18602

A dome-shaped opening, a smooth membrane phase, and microfibrils could all be seen in the SEM image of pure chitosan in Figure 4b (Leudjo Taka *et al.*, 2021). Figure 4c displays the composites' SEM images. The porous surface of the nanocomposites, which is brought between the CNCs chains and the grafted chitosan structure, there are physical crosslinking sites, which may be seen in SEM images of the materials. This permeable setting can accelerate the enlargement of nanocomposites by expanding the liquid's swelling contact surface area (Shojaeiarani *et al.*, 2019).

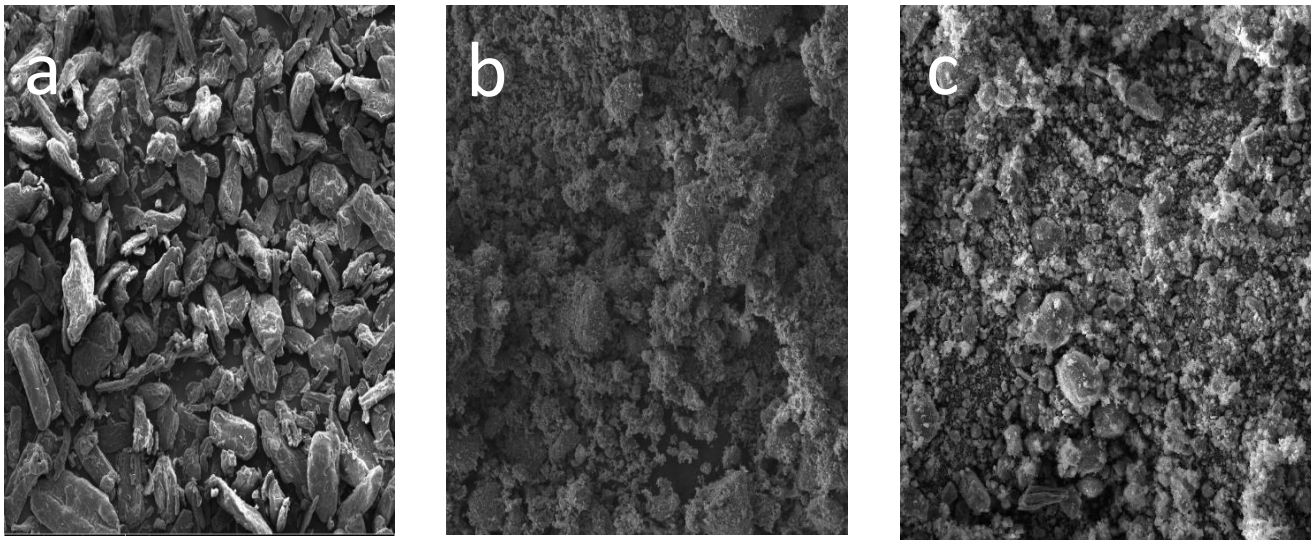

Figure 4. *The scanning electron microscope image of (a) cellulose nanocrystals, (b) pure chitosan, (c) composites.*

Figure 5 shows the thermogravimetric analyzer graphs of samples made of the CNCs, chitosan, and composites in a nitrogen environment, heated at an average rate of 15 °C min^{-1}. The first degradation occurs between 20 and 100 °C due to the materials' residual water evaporating, resulting in 5% weight losses CNCs and chitosan each and 10% weight loss for the nanocomposite, respectively. The next phase of degradation was noticed at higher temperatures as a result of the CNCs-chitosan's thermal degradation. CNCs lost weight quickly between 250 and 300 °C, then gradually between 300 and 400 °C. A noticeable deterioration peak between 252 and 403 °C is associated with the disintegration of the cellulose rings.(Moharrami & Motamedi, 2020) The second stage featured a weight reduction of 70% from 250°C to 350°C. In the third stage, there was a 7% weight loss over 400°C. In phases two and three, weight loss is correlated with the depolymerization, disintegration, and deconstruction of the acetylated units of chitosan and chitosan itself.(Zhang *et al.*, 2016) Around 250°C, nanocomposites started to degrade, comparable to the breakdown of CNCs and Chitosan, proving the efficiency of the synthesis process.

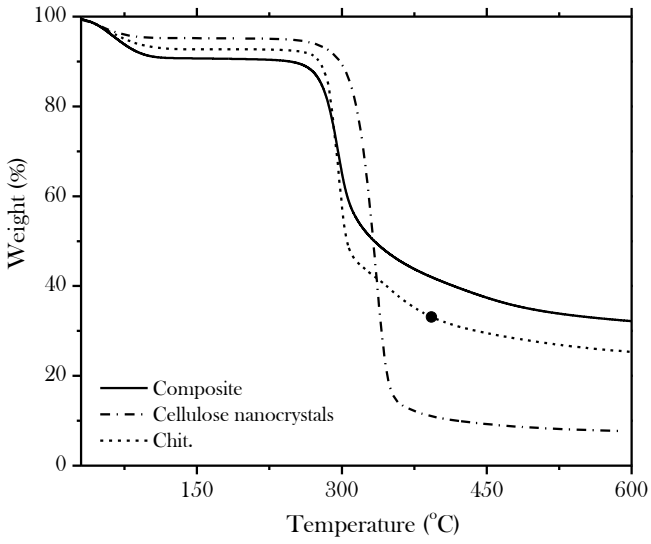

Figure 5. *The thermogravimetric analyzer graphs of composite, cellulose nanocrystals, and Chitosan*

EQA 60 (2024): 1-17

DOI: 10.6092/issn.2281-4485/18602

The Brunauer-Emmett-Teller analysis determined the exact surface area of the nanocomposites, chitosan, and CNCs(Table 2). It can be seen that the distribution of surface area and the breadth of the pore volume follow an ascending order: Nanocomposites > CNCs > Chitosan. Adding urea molecules during the nanoparticle modification procedure enhanced the nanocomposites' surface area and pore volume. The urea increased N_2 diffusion across numerous main CNCs and chitosan channels, widening their pore dimensions and surface area.

Material	surface area (m^2/g)	Pore dimension (cm^3/g)
Cellulose nanocrystals	2.396	0.003
Chitosan	2.587	0.002
Nanocomposites	5.945	0.021

Table 2 *The Brunauer-Emmett-Teller results of chitosan, cellulose nanocrystals, and composite*

Table 3. *The experimental data and independent variables for adsorption of* Cd^2

Run	Y_2: Time (min)	Y_1: pH	Y_4:Initial conc. (mg/L)	Y_3: Dosage (mg/L)	q_e Experimental (mg/g)	q_e Predicted (mg/g)	Residual
1	0	0	0	0	319.01	317.71	1.29
2	0	0	+1	0	289.06	290.91	-191
3	+1	+1	-1	-1	432.05	432.77	-0.77
4	+1	+1	+1	-1	369.00	368.5	0.48
5	+1	-1	-1	+1	422.03	422.77	-0.76
6	+1	0	0	0	379.05	378.41	0.59
7	0	0	0	0	316.06	317.71	-1.71
8	0	0	0	+1	202.01	202.77	-0.77
9	+1	-1	+1	+1	300.02	299.52	0.49
10	-1	+1	+1	+1	40.07	39.52	0.48
11	0	+1	0	0	235.01	2.34.41	0.59
12	-1	-1	+1	-1	141.02	140.52	-0.77
13	-1	0	0	0	185.03	184.41	0.59
14	-1	-1	-1	-1	202.05	202.77	0.58
15	0	0	0	0	317.06	317.71	-0.71
16	-1	+1	-1	+1	133.02	133.77	-0.78
17	0	0	0	0	315.03	317.71	-1.70
18	0	0	0	0	318.08	317.71	0.29
19	0	0	0	-1	390.02	389.41	0.59
20	0	0	-1	0	380.03	376.91	3.09
21	0	0	0	0	255.02	254.41	0.57

The RSM modelling. Considering previous studies (Aden *et al.*, 2017; Chen *et al.*, 2019; Ihsanullah *et al.*, 2016; Nordin *et al.*, 2021; Oyewo *et al.*, 2019; Tang *et al.*, 2016; Vishnu Priyan *et al.*, 2021), the initial pH, time, dosage, cadmium ions concentration, and adsorbent dosage were selected as independent factors. The outcome of the experiment was the adsorption capacity (qe). Three levels were used to select the experimental runs' order at random. There were twenty-one runs in the experimental design,. and each experiment was repeated. Using a central composite design, the effectiveness of Cd^{2+} adsorption was investigated. Table 3 lists the experimental strategy and the outcomes that were attained.

Model fitting and ANOVA analysis. Table 4 shows the ANOVA findings for the developed quadratic RSM. The generated solution surface quadratic equation's statistical approximation of the Cd^{2+} removal on the developed composite was tested using the ANOVA approach.

DOI: 10.6092/issn.2281-4485/18602

The equation's relevance is reflected by its F-value of 2843.43. P-values for significant model terms are less than 0.0001. The important model terms are: Y_1, Y_3, Y_4, Y_2Y_4, Y_3Y_4, Y_1^2, Y_2^2, Y_4^2. P-values greater than 0.1 indicate that a model parameter is not significant. The p-value indicates the probability of rejecting the null hypothesis. Each coefficient is more crucial; the higher the Fisher's F-value, the more precise the model is.(Shahnaz *et al.*, 2020) According to the p-value for lack of fit, which is more than 0.05, the model fits the experimental data, and the indepen-dent process variables significantly impact the response. The coefficients of a certain process variable and two combination variables explain the amount of the variable's influence and the intera-ction between the two variables.(Derikvandi & Nezamzadeh-Ejhieh, 2017) The most influential parameters on the model according to F-value: $Y_1 > Y_3 > Y_2^2 > Y_1^2 > Y_4 > Y_2Y_4 > Y_3Y_4 > Y_3^2 > Y_2 > Y_1Y_2 > Y_1Y_3 > Y_2Y_3 > Y_1Y_4$. It was shown that the initial Cd^{2+} concentration and the dosage of the adsorbate had the most impact on the model. There was a substantial correlation between the anticipated and experimental responses, as indicated by the coefficient of determination (R^2) of 0.989, Predicted R^2 of 0.992, and adjusted R^2 of 0.987, which measures the degree of fitness. These figures are close to one, indicating that the model is viable. The quadratic model equation in Equation [3] depicts how the independent process elements impact the response of Cd^{2+} removal efficiency.

$$q_e = 370.71+97.00Y_1- 10.10Y_2- 43.01Y_3 - 40.90Y_4 - 36.29Y_1^2- 72.29Y_2^2+ 15.99Y_3^2+ 30.69Y_4^2- 9.79Y_1Y_2- 3.90Y_1Y_3 + 1.37\ Y_1Y_4+ 3.36Y_2Y_3 - 28.77Y_2Y_4- 11.29\ Y_3Y_4 \quad [3]$$

The above model equation can be simplified by eliminating the unimportant terms. The residuals' standard probability plots (average percent probability vs. internally studentized residuals) indicate no noticeable divergence from the norm (Fig. 6).

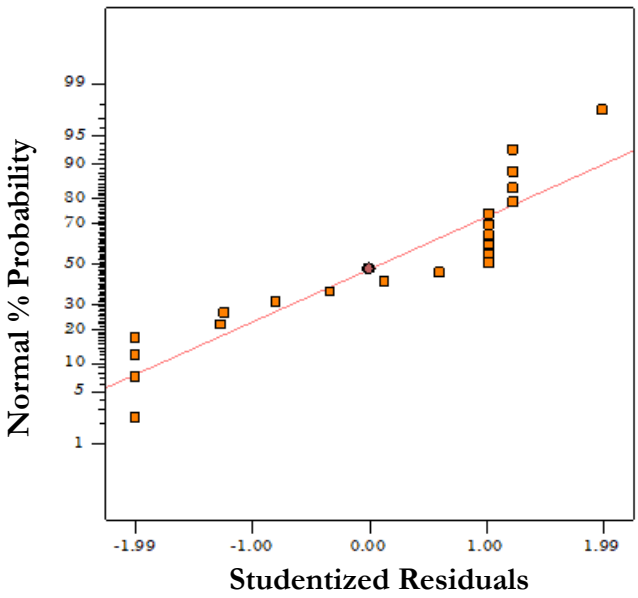

Figure 6. *The studentized and average percentage probability residuals for Cd2+removal.*

Parameters	value	Error	Value (F)	Value (P)	
model	317.71	0.75	2843.43	<0.0001	significant
Y_1	97.00	1.61	3633.42	<0.0001	
Y_2	-10.00	1.61	38.62	0.0008	
Y_3	-43.00	0.72	3570.09	<0.0001	
Y_4	-41.00	1.61	649.14	<0.0001	
Y_1^2	-36.30	1.42	649.36	0.0005	
Y_2^2	-73.30	1.42	2648.07	<0.0001	
Y_3^2	16.20	1.42	129.42	0.0005	
D^2	30.70	1.42	464.68	<0.0001	
Y_1Y_2	-9.88	1.80	30.13	0.0015	
Y_1Y_3	-3.88	0.80	23.19	0.0475	
Y_1Y_4	1.38	1.80	0.58	0.0014	
Y_2Y_3	3.37	0.80	17.59	0.0005	
Y_2Y_4	-28.87	1.80	257.58	<0.001	
Y_3Y_4	-11.37	0.80	199.86	<0.001	
Lack of fit			10.54	4.21	Not significant

Table 4
ANOVA

DOI: 10.6092/issn.2281-4485/18602

Response surface plots

Figure 7(a) shows pH and dosage as elliptic contour plots. From the figures, the circular nature contour plot demonstrates how dose and pH significantly impact adsorbent capacity. The adsorbent increased to pH 5 and a 5 mg/L dose. The reaction halted when the pH was >6 and the dosage was >20 mg/L. This could be because cationic species can impede the movement of such ions toward the surface in nanocomposite locations. Higher pH values may cause cadmium to precipitate as $Cd(OH)_2$, which has a decreased adsorption capability. The removal of Cd^{2+} from the solution depends on contact duration and concentration

As seen in Figure 7(b), the solution/solid interface, dose, and adsorption capacity of nanocomposites may all be affected by the contact time of the solution.(Musikavanhu *et al.*, 2019) The shape of the contour reveals how the nanocomposite's interaction and duration of contact are more significant than the starting concentration. The length of any interactions is a crucial consideration in all processes. The adsorbate, Cd^{2+}, was better absorbed with longer contact times and higher starting concentrations. Due to the availability of more active sorption sites and enough contact time for the adsorption process, Cd^{2+} removal has become more effective.(Chen *et al.*, 2019).

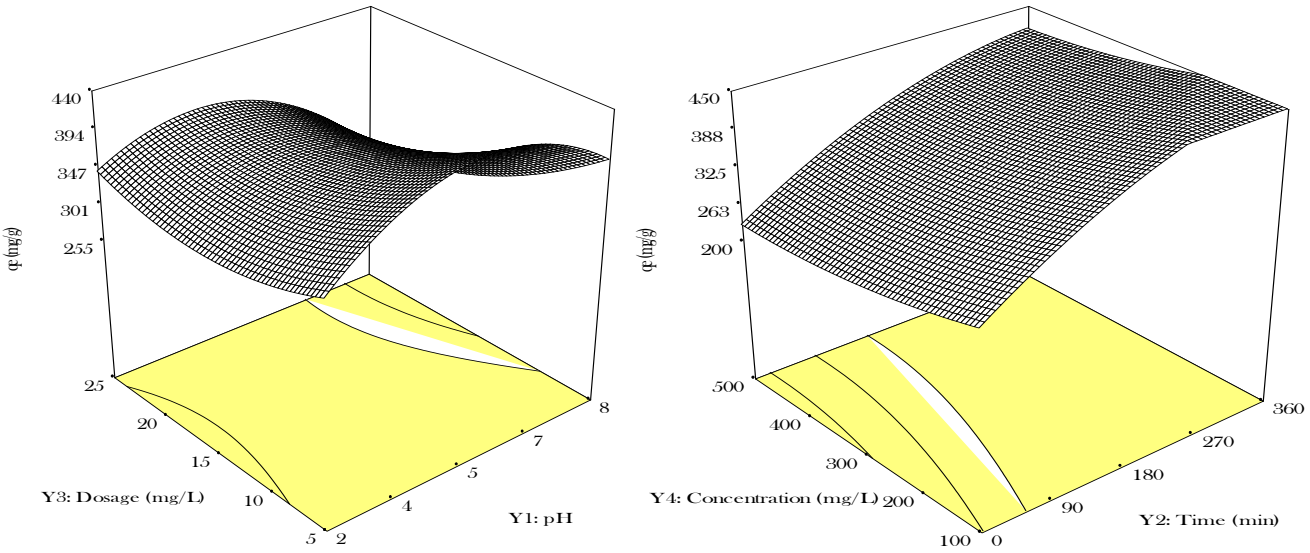

Figure 7. *a)The 3D surface (a) the effect of pH and dosage; b) the effect of time and concentration on the Cd^{2+}removal efficiency using nanocomposites at constant time and concentration.*

As seen in Figure 8, the perturbation plot depicts how process factors affect adsorption capacity. The adsorption capacity, while the other factors stayed constant, was assessed and shown alongside the impact of one element. The perturbation plot shows that the adsorption capacity rises when contact time and pH rise to 6. The variance analysis (ANOVA) and the result accord exactly.

ANN (Artificial neural network) modeling

The RSM data sets obtained were tripled. This yielded sixty-three (63) data sets, which were enough for the Artificial neural network investigation. Consequently, the ANNs are used to create new

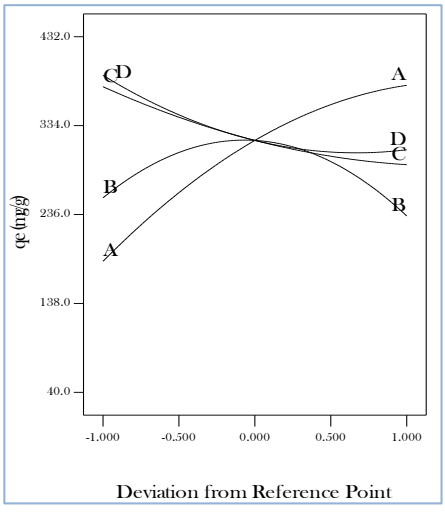

Figure 8
The perturbation plot.

DOI: 10.6092/issn.2281-4485/18602

processes, evaluate existing ones, and forecast the results and behavior of systems.(Aversano *et al.*, 2021) In most cases, the back-propagation approach is used to instruct MLPs. MLP networks can employ the Levenberg-Marquardt (LM), gradient descent (GD), and conjugate gradient (CG) approaches to reduce errors. The experiments created by the Central Composite Design provided the input information and training data. The data was selected, a network was built, and it was trained using the Neural Fitting tool. The MATLAB(The Math Works Inc. 2015a) program's mean square error (MSE) and regression analysis coefficient (R^2) were used to evaluate its performance. The MLP network was trained using the Levenberg-Marquardt backpropagation technique (4:10:1). Generally, this method is quicker but uses more memory. This occurs when the MSE of the validation samples increases, and generalization stops improving. The optimal total number of neurons for the hidden layer, the optimal number of cases for developing and validating the model, and the optimal number of samples for testing the model may all be determined using this method. There were 63 samples overall used for the ANN modeling, of which 10%, 15%, and 75% were used for validating, testing, and training, respectively. Several neurons were selected by trial and error methods for the concealed layer, and the best number was then trained for seven iterations. R^2, the average regression coefficient, was discovered to be 0.999. Figure 9 displays the performance and regression graphs of the trained network.

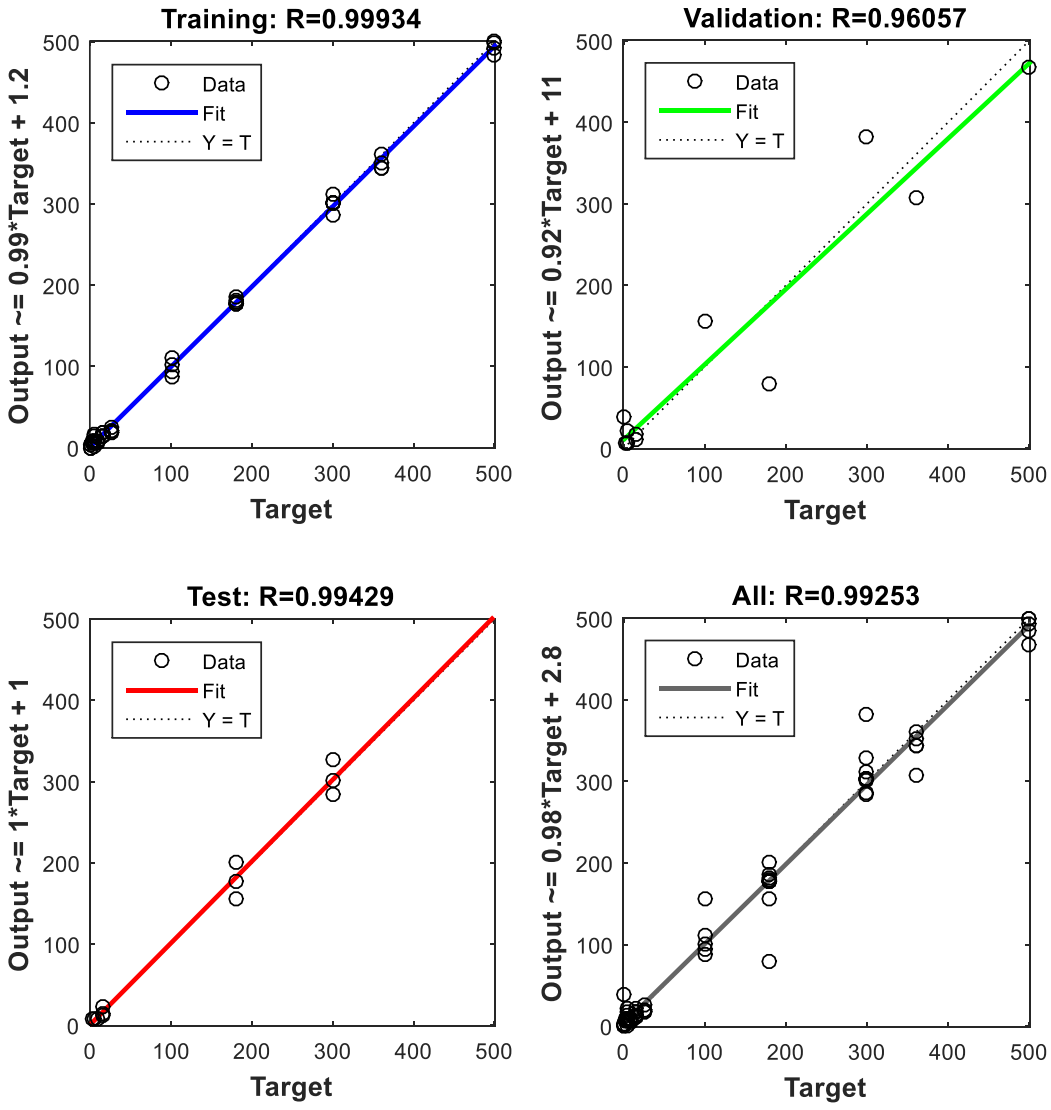

Figure 9.
Results of the regression evaluation for the artificial neural network output.

DOI: 10.6092/issn.2281-4485/18602

Comparison RSM-ANN

Using RMSE, SSE, HYBRID, MPSD, SAE, MSE, R^2, AAD, ARE, and X^2 (Equations 4–11) were used to evaluate the performance and choose the optimum modeling approach for expecting output responses.

$$\text{The chi-square} = \frac{(q_e - q_{e(calc)})^2}{q_e} \quad [4]$$

$$\text{The RMSE} = \sqrt{\frac{1}{n}\sum_{i=1}^{n}\left(\frac{(q_e - q_{e(calc)})^2}{q_e}\right)} \quad [5]$$

$$\text{The ARE} = \sum_{i=1}^{n}(q_e - q_{e(calc)})^2 \quad [6]$$

$$\text{The SAE} = \sum_{i=1}^{n}[(q_e - q_{e(calc)})] \quad [7]$$

$$\text{The HYBRID} = \frac{1}{n-q}\sum_{i=1}^{n}\left(\frac{(q_e - q_{e(calc)})^2}{q_e}\right)x100 \quad [8]$$

$$\text{The SSE} = \frac{100}{n}\sum_{i=1}^{n}\left([\frac{(q_e - q_{e(calc)})^i}{q_e}]\right) \quad [9]$$

$$\text{The MSE} = \frac{1}{n}\sum_{i=1}^{n}(q_e - q_{e(calc)})^2 \quad [10]$$

$$\text{MPSD} = 100\sqrt{\frac{1}{n-q}\sum_{i=1}^{n}\left(\frac{(q_e - q_{e(calc)})^2}{q_e}\right)i} \quad [11]$$

Table 5 displays the linear error function for the Response surface method and Artificial neural network. The lowest possible error functions represent the best fits. Due to its lower error function values, the RSM model is preferable to the ANN model. It may be a result of the fact that the current study only used a few experimental runs. The ANN often needs numerous data points to function well during network training (Aversano *et al.*, 2021; Dolatabadi *et al.*, 2018; Franco *et al.*, 2020). The actual and forecasted data for RSM and ANN are shown in Fig. 10. As demonstrated in Table 6, The adsorption of Cd^{2+} from the produced composite was accurately predicted by the RSM model. The RSM was used to optimize the Cd^{2+} adsorption on nanocomposites.

Table 5. *Error functions for ANN and RSM*

Error function	ANN	RSM
X^2	0.008	0.001
ADD	0.006	0.004
MSE	0.0002	0.0001
ARE	2.982	2.543
HYBRID	0.0035	0.0012
R^2	0.993	0.997
SAE	0.096	0.094
SSE	0.138	0.121
MPSD	0.538	0.413
RMSE	0.0011	0.0005

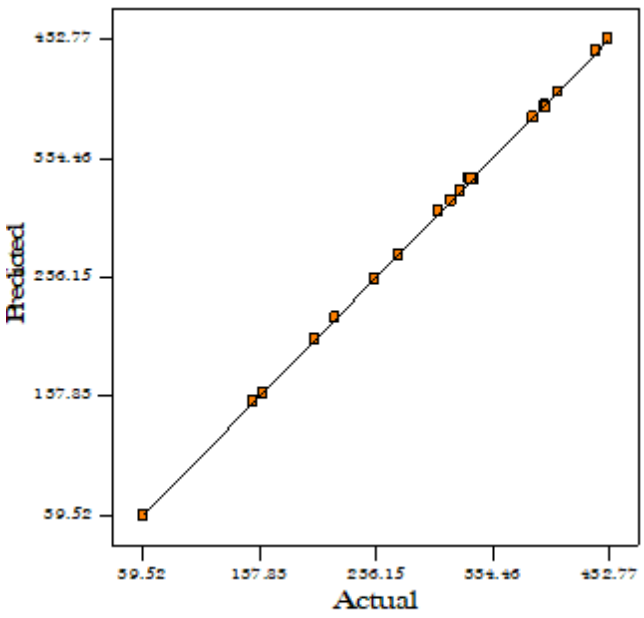

Figure 10. *RSM comparison of expected and actual results*

Y_1	Y_2	Y_3	Y_4	q_e(calc)	RSM q_e (calc)	ANN q_e(calc)
3.71	294	16.01	15.70	340.23	340.96	338.63
5.09	265	13.15	12.14	320.35	320.53	319.36
3.96	162	11.39	10.65	311.08	310.98	312.04
4.52	244	19.63	15.62	388.78	388.70	389.96

Table 6
Cd^{2+} removal using ANN and RSM techniques, actual and predicted values

DOI: 10.6092/issn.2281-4485/18602

Numerical Optimization Centrale Composite Design (RSM)

Table 7 concisely summarizes the ideal circumstances for Cd^{2+} adsorption on the nanocomposites. The ideal conditions resulted in an experimental adsorption capacity of 440.01 mg/g. 440.05 mg/g was found to be the adsorption capacity, which aligns with the forecast. A developed model is considered satisfactory when the target value is close to 1. The model is frequently used and desired, as shown by the value 1.

Table 7. *The optimal predicted condition for the highest Cd^{2+} adsorption on the composite.*

Y_1	Y^2	Y_3	Y_4	q_e adsorption capacity	Desirability
5.64	315	16.93	333.96	440.01	0.999
4.94	354	17.48	320.23	440.05	0.999

Isotherm and kinetics of Cd^{2+}adsorption

Adsorption isotherms define the interaction and maximum adsorption capacity of adsorbate and adsorbent. Experimental data is fitted to Dubinin-Radushkevich, Temkin, Langmuir, and Freundlich isotherm models to perform equilibrium investigations (Kabuba & Banza, 2020). The fitted model was verified using error functions (X^2) and regression analysis (R^2). Table 8 displays the findings. As can be shown, the Langmuir model has the lowest error function (0.011) and most significant correlation coefficients ($R^2 > 0.995$). This means that the Langmuir model is suitable, as shown by this result. Compared to the Freundlich, D-R, and Temkin isotherm models, it can be regarded as the most accurate technique to characterize the Cd^{2+} adsorption process on the nanocomposites. The Cd^{2+} was adsorbed onto the composite in a single-layered way, and the active sites on the material's

Table 8. *Cd^{2+} adsorption onto composite under RSM-optimized conditions, regression coefficients, kinetic parameters, and isotherm model.*

Models	Formula	Variables	values	X^2
Langmuir	$\frac{C_{final}}{q_e} = \frac{C_{final}}{q_m} + \frac{1}{Cq_m}$	R^2	0.997	0.009
		q_{ma}(mg/g)	438.02	
		C (Lmg^{-1})	0.821	
Temkin	$q_e = X \ln C_{final} + K_{tem}$	R^2	0.823	0.035
		K_{tem}	310.63	
		X	8.235	
Freundlich	$\text{Log } q_{ex} = \log K_{freud} + \frac{1}{n}\log C_{final}$	R^2	0.954	0.049
		K_f (Lmg^{-1})	299.25	
		n	6.149	
Dubini-Radushkevich	$\ln q_{ex} = \ln q_{maximum} - bA^2$	R^2	816.715	0.039
	$A = RT \ln(1 + \frac{1}{C_{eq}})$	E ($Kj.mol^{-1}$)	0.875	
		b (mol^2j^2)	$2.366.10^{-9}$	
Pseudo first-order	$\text{Log } (q_{ex}\text{-}q_{tm}) = \log q_{ex} - \frac{K_{first}}{2.3}t$	R^2	0.972	0.025
		K_{first} (min^{-1})	0.0279	
		q_{ex} (mg/g)	258.962	
Pseudo second-order	$\frac{t}{q_t} = \frac{1}{K_S q_{ex}^2} + \frac{1}{q_{ex}}t$	R^2	0.997	0.013
		q_{ex}(mg/g)	376.325	
		K_S (g/mg.min^{-1})	0.157	
Elovich	$q_t = \frac{1}{D}\ln aD + \frac{1}{D}\ln t$	R^2	0.989	0.062
		a(g/mg.min^{-1})	0.025	
		D (g/mg)	9.521	
Intraparticle diffusion	$qt = K_{diffusion}\, t^{0.5} + E$	R^2	0.923	0.037
		E	0.018	
		K(g/mg.$min^{1/2}$)	2.185	

EQA 60 (2024): 1-17

DOI: 10.6092/issn.2281-4485/18602

adsorbent interface were equally distributed, as suggested by the Langmuir isotherm model. The physical and chemical characteristics of the reaction may be predicted using the mean adsorption energy, E. Physical adsorption happens when E is less than 8 kJ mol-1; chemical adsorption happens when E is between 8 and 16 kJ mol-1; and chemical adsorption happens when E is larger than 20 kJ mol-1. The Cd^{2+} adsorption onto the adsorbent is a chemisorption process because E was greater than 8 kJ mol^{-1}, according to the Dubini-Radushkevich model.

In order to fit and correlate the results of the experiments, pseudo-first-order and pseudo-second-order kinetic approaches were employed. To explore the mass transfer rate and mechanism of the adsorption process together with Elovich intraparticle diffusion. The lower agreement between qe (actual) and qe (predicted), as well as the higher correlation coefficient (R^2 > 0.997), indicate the pseudo-second-order model's capability to explain the experimental findings. Then, an intraparticle diffusion model built on the Weber and Morris theories was used to assess the kinetic findings. According to the Morris hypothesis, an adsorption process is exclusively governed by intraparticle diffusion, as seen by a qt vs. $t^{0.5}$ linear line with an A = 0 slope. The rate is influenced by more than only pore diffusion and adsorption. The C values describe the thickness of the boundary layer. The intercept (B value) increases with increasing border size. The maximum Cd^{2+} adsorption ability of composite and various adsorbing materials is evaluated in Table 9. The composite showed high and satisfactory ability to remove Cd^{2+} from the aqueous medium compared to standard sorbents.

Table 9
Adsorbent capacity comparison

Sorbent	q_{max} (mg/g)	Reference
Modified CNCs Amino	135.06	(Azad et al., 2021)
CNCs with succinic acid	250.07	(Igberase et al., 2014)
Chitosan	144.01	(Chen et al., 2019)
Nanocomposites	52.80	(Oyewo et al., 2019)
Cellulose modified	400.01	(Oyewo et al., 2019)
Composite	438.02	This research

The investigation of binding capacity

According to a mechanistic investigation, the composite has more active adsorption sites and a greater capacity for adsorption. Quantum chemical modeling was used to determine better The most effective place for adsorption, and the energy of attraction between the adsorption materials and Cd^{2+} should be identified. By employing glucose as the fundamental building block, cellulose was made simpler. Three kinds of cellulose modified with distinct functional groups were constrained to study and compare their contributions. Table 10 displays energy information as well as stability Cd^{2+} adsorption configurations on the material. The ability of the adsorbent to bind Cd^{2+} increases as the absolute quantity of binding energy rises. The order of the bond capacity was CNCs, carboxyl-CNCs, and Amide-CNCs. The cellulose nanocrystals-amide demonstrated the strongest capacity to bind compared to the unprocessed CNCs. The most effective adsorbents for binding have more than one functional group change. It was caused by the solid

Matrix	H_{OMO} Eg	L_{UMO} Eg	Eg Kcal.mol^{-1}	E Kcal.mol^{-1}
CNC	-0.240	-0.298	47.8	-67.3
R-COOH—CNC	-0.233	-0.298	46.7	-72.2
CO-NH—CNC	-0.214	-0.298	59.1	-80.7

Table 10
The Energy differences and the bonding force between the adsorbent material and Cd^{2+}.

DOI: 10.6092/issn.2281-4485/18602

capacity of the N soliton to donate electrons (Wang *et al.*, 2021).

In the nanocomposite, the functional groups are crucial for synergistic adsorption. The adsorbent may be considered chemisorbing during the electron transition between the L_{UMO} and H_{OMO} of Cd^{2+}. Table 10 displays the H_{OMO} consisting of multiple cellulose adsorption agents modified with chemical groups, the L_{UMO}, and the energy differential between the absorbent material and the Cd^{2+}. The probability of a spontaneous electronic transition occurring rises as the energy gap widens, and the adsorbent utilized has a larger adsorption capacity. The difference in energy was largest in the multifunctionally improved CNCs, which may have been caused by the breakdown between H and CO-NH from the cellulose and chitosan, which opened up more active locations for adsorption and increased the adsorbent's ability to attract Cd^{2+}.

Conclusions

The efficiency of the composite in removing Cd^{2+} from wastewater and the impact of operational parameters on the adsorption capacity in a batch process was assessed using the response surface method and artificial neural network. The results showed that nanocomposites were more thermally stable than CNCs and chitosan, and FTIR analysis confirmed that the composites' functional groups were equivalent to those of CNCs and chitosan. The nanocomposites' SEM pictures revealed a porous structure, thin particle size, and needle-like shape. These results showed that the nanocomposites could filter out metal ions from wastewater. The interactions of the process variables and their optimal conditions were studied. The adsorption capacity of 440.01 mg/g was found to be optimum with a pH of 5.65, starting concentration of 333 mg/L, contact duration of 315 minutes, and dosage adsorbent of 16.93 mg. According to validation information, the outcomes of two approaches, ANN and RSM suggested that RSM with R^2 of 0.997 and ANN with R^2 of 0.993 are reliable and exact techniques for predicting the adsorption process. The Freundlich and Temkin isotherms did not correspond to the equilibrium data, as well as the Langmuir isotherm. According to the D-R model, the energy required for Cd^{2+} adsorption is larger than 8 kJ mol-1, suggesting that chemisorption is the mechanism involved. The adsorption kinetics were properly predicted using the pseudo-second-order rate model. A multifunctional grafted cellulose nanocrystals derivative adsorbent (nanocomposites) with carboxyl, amide, and secondary amino groups was successfully created for Cd^{2+} removal. Additionally, the functional groups cooperate to allow Cd^{2+} to bind to the nanocomposites.

Abbreviation

ANN: Artificial neural network.
CNCs: Cellulose nanocrystals
CCD: Central Composite Design
D-R: Dubini-Radushkevich
RSM: Response Surface Methodology
RMSE: Root means square errors
SSE: sum squared errors
HYBRID: Hybrid fractional error function
MPSD: Derivative of Marquardt's percent standard deviation
SAE: sum absolute errors
MSE: Mean square errors
X^2: Chi-square
AAD: Absolute average deviation
ARE: Average relative errors
HOMO: Highest occupied molecular orbital
LUMO: Lowest occupied molecular orbital

Data Availability

The data supporting this study's findings are available on request from the corresponding author. The data are not publicly available due to privacy or ethical restrictions.

Author Contribution

Banza Jean Claude: conceptualization, methodology, formal analysis, investigation, data curation, writing, writing- original draft - Maurice Stephane Onyango: formal analysis, validation, formal analysis, investigation, writing-reviewing, and editing.

Acknowledgments

The Tshwane University of Technology is acknowledged for providing facilities.

Declaration Of Competing Interest

The authors declare that they have no known competition for financial interests or personal relationships that could have influenced the work reported in this paper.

DOI: 10.6092/issn.2281-4485/18602

References

ADEN M., UBOL R.N., KNORR M., HUSSON J., EUVRARD M. (2017) Efficent removal of nickel(II) salts from aqueous solution using carboxymethylchitosan-coated silica particles as adsorbent. Carbohydrydrate Polymers 173:372–382. https://doi.org/10.1016/j. carbpol. 2017.05.090

AHMADI, S., MESBAH, M., IGWEGBE, C.A., EZELIORA, C.D., OSAGIE, C., KHAN, N.A., DOTTO, G.L., SALARI, M., & DEHGHANI, M.H. (2021) Sono electro-chemical synthesis of $LaFeO_3$ nano-particles for the removal of fluoride: Optimization and modeling using RSM, ANN and GA tools. Journal Environmental Chemical Engineering 9(4):105320. https://doi.org/10.1016/j.jece.2021.105320

AKHTAR A., AKRAM K., ASLAM Z., IHSANULLAH I., BAIG N., BELLO M.M. (2022) Photocatalytic degradation of p-nitrophenol in wastewater by heterogeneous cobalt supported ZnO nanoparticles: Modeling and optimization using response surface methodology. *Environmental Progress Sustainaible Energy.* https://doi.org/10.1002/ep.13984

AVERSANO G., D'ALESSIO G., COUSSEMENT A., CONTINO F., PARENTE A. (2021) Combination of polynomial chaos and Kriging for reduced-order model of reacting flow applications. Results Engineering 10: 100223. https://doi.org/10.1016/j.rineng.2021.100223

AYOOLA A.A., HYMORE F.K., OMONHINMIN C.A., OLAWOLE O.C., FAYOMI O.S.I., BABA-TUNDE D., FAGBIELE O. (2019) Analysis of waste groundnut oil biodiesel production using response surface methodology and artificial neural network. Chemical Data Collection 22:100238. https://doi.org/10.1016/ j.cdc.2019.100238.

AZAD H., MOHSENNIA M., CHENG C., AMINI A. (2021) Facile fabrication of PVB-PVA blend polymer nano composite for simultaneous removal of heavy metal ions from aqueous solutions: Kinetic, equilibrium, reusability and adsorption mechanism. Journal Environmental Chemical Engineering. 9(5):106214. https://doi.org/10.1016/j.jece.2021.106214

BOHLOULI A., AFSHAR M.R., ABOUTALEBI M.R., SEYEDEIN S.H. (2016) Optimization of tungsten leaching from low manganese wolframite concentrate using Response Surface Methodology (RSM). International Journal Refractory Metal Hard Material 61:107–114. https://doi.org/10.1016/j.ijrmhm.2016.07.012

CHEN Q., ZHENG J., WEN L., YANG C., ZHANG, L. (2019) A multi-functional-group modified cellulose for enhanced heavy metal cadmium adsorption: performance and quantum chemical mechanism. Chemosphere. 224:509–518. https://doi.org/10.1016/j.chemosphere. 2019.02.138.

CHENG K., HUANG C., WEI Y., HSU S. (2019) Novel chitosan – cellulose nano fi ber self- healing hydrogels to correlate self-healing properties of hydrogels with neural regeneration effects. NPG Asia Material. https://doi.org/10.1038/s41427-019-0124-z

COJOCARU C., HUMELNICU A.C., PASCARIU P., SAMOILA P. (2021) Artificial neural network and molecular modeling for assessing the adsorption performance of a hybrid alginate-based magsorbent. Journal Molecular Liquids. 337:116406. https://doi.org/ 10.1016/j.molliq.2021.116406

DERIKVANDI H., NEZAMZADEH-EJHIEH A. (2017) Designing of experiments for evaluating the interactions of influencing factors on the photocatalytic activity of NiS and SnS2: Focus on coupling, supporting and nanoparticles. Journal Colloid Interface Science. 490:628–641. https://doi.org/10.1016/j.jcis.2016.11.102

DESHWAL S., KUMAR A., CHHABRA D. (2020) Exercising hybrid statistical tools GA-RSM, GA-ANN and GA-ANFIS to optimize FDM process parameters for tensile strength improvement.*CIRP J.* Manufacture Science Technology. 31:189–199. https://doi.org/10.1016/ j.cirpj.2020.05.009.

DOLATABADI, M., MEHRABPOUR, M., ESFANDYARI, M., ALIDADI, H., & DAVOUDI, M. (2018) Modeling of simultaneous adsorption of dye and metal ion by sawdust from aqueous solution using of ANN and ANFIS. Chemometrics Intelligent Laboratory Systems 181:72–78. https://doi.org/10.1016/ j.chemolab. 2018.07.012.

FRANCO D.S.P., DUARTE F.A., SALAU N.P.G., DOTTO G.L. (2020) Analysis of indium (III) adsorption from leachates of LCD screens using artificial neural networks (ANN) and adaptive neuro-fuzzy inference systems (ANIFS). Journal Hazardous Materials. 384:121137. https://doi.org/10.1016/j.jhazmat.2019.121137.

HENSCHEN J., LI D., EK M. (2019) Preparation of cellulose nanomaterials via cellulose oxalates. Carbohydrate Polymers. 213:208–216. https://doi.org/10.1016/ j.carbpol. 2019.02.056.

IGBERASE E., OSIFO P., OFOMAJA A. (2014) The adsorption of copper (II) ions by polyaniline graft chitosan beads from aqueous solution: Equilibrium, kinetic and desorption studies. Journal Environmental Chemical Engineering, 2(1):362–369. https://doi.org/ 10.1016/j.jece.2014.01.008.

DOI: 10.6092/issn.2281-4485/18602

IHSANULLAH ABBAS A., AL-AMER A.M., LAOUI T., AL-MARRI M.J., NASSER M.S., KHRAISHEH M., ATIEH M.A. (2016) Heavy metal removal from aqueous solution by advanced carbon nanotubes: Critical review of adsorption applications. Separation Purification Technology, .157:141–161. https://doi.org/10.1016/j.seppur. 2015.11.039

KABUBA J., BANZA M. (2020) Results in Engineering Ion-exchange process for the removal of Ni (II) and Co (II) from wastewater using modi fi ed clinoptilolite : Modeling by response surface methodology and arti fi cial neural network. Results Engineering. 8:100189. https://doi.org/10.1016/j.rineng.2020.100189

KHADHRI N., EL M., SAAD K., MOUSSAOUI Y. (2019) Journal of Environmental Chemical Engineering Batch and continuous column adsorption of indigo carmine onto activated carbon derived from date palm petiole. Journal Environemental Chemical Engineering, 7(1):102775. https://doi.org/10.1016/j.jece.2018.11.020

LEUDJO TAKA A., KLINK M.J., YANGKOU MBIANDA X., NAIDOO E.B. (2021) Chitosan nanocomposites for water treatment by fixed-bed continuous flow column adsorption: A review. Carbohydrate Polymers. 255:117398. https://doi.org/10.1016/j.carbpol.2020.117398.

MASEKELA D., HINTSHO-MBITA N.C., MABUBA N. (2022) Diethylamine functionalised Moringa oleifera leaves for the removal of chromium(VI) and bacteria from wastewater. International Journal Environmental Analytical Chemistry,102(13):3002–3022. https://doi.org/10.1080/03067319.2020.1762873.

MO C., ZHANG Q., LI H., YANG Z., XU H., HUANG G., QU A., CHEN Y. (2021) Enhanced photodegradation ability and mechanism study of g-C3N4 by dual modified with sulfur-containing quantum dots doping after oxidization. Journal Photochemical Photobiology A Chemical. 419:113462. https://doi.org/10.1016/j.jphotochem.2021.113462

MOHARRAMI P., MOTAMEDI E. (2020) Application of cellulose nanocrystals prepared from agricultural wastes for synthesis of starch-based hydrogel nanocomposites: Efficient and selective nanoadsorbent for removal of cationic dyes from water. Bioresource Technology Elsevier. 313:123661. https://doi.org/10.1016/j.biortech.2020.123661.

MUSIKAVANHU B., HU Z., DZAPATA R.L., XU Y., CHRISTIE P., GUO D. (2019) Applied Surface Science Facile method for the preparation of superhydrophobic cellulosic paper. Applied Surface Science. 496:143648. https://doi.org/10.1016/j.apsusc.2019.143648

NORDIN A.H., WONG S., NGADI N., ZAINOL M.M., AIEN N., ABD F., NABGAN W. (2021) Journal of Environmental Chemical Engineering Surface functionalization of cellulose with polyethyleneimine and magnetic nanoparticles for efficient removal of anionic dye in wastewater. Journal Environmental Chemical Engineering. 9(1):104639. https://doi.org/10.1016/j.jece. 2020.104639.

OLAD A., DOUSTDAR F., GHAREKHANI H. (2020) Fabrication and characterization of a starch-based superabsorbent hydrogel composite reinforced with cellulose nanocrystals from potato peel waste. Colloids Surfaces A Physicochemical Engineering Aspect. 601: 124962. https://doi.org/10.1016/j.colsurfa.2020. 124962.

OLATUNJI O.M., HORSFALL I.T., ONUOHA-UKOHA E., OSA-ARIA K. (2022) Application of hybrid ANFIS-based non-linear regression modeling to predict the %oil yield from grape peels: Effect of process parameters and FIS generation techniques. Clean Engineeering Technology. 6:100371. https://doi.org/10.1016/j.clet.2021.100371.

OYEWO O.A., MUTESSE B., LESWI T.Y., ONYANGO M.S. (2019) Journal of Environmental Chemical Engineering Highly efficient removal of nickel and cadmium from water using sawdust- derived cellulose nanocrystals. 7(4):103251. https://doi.org/10.1016/j.jece.2019.103251.

PRIYA E., KUMAR S., VERMA C., SARKAR S., MAJI, P.K. (2022) A comprehensive review on technological advances of adsorption for removing nitrate and phosphate from waste water. Journal Water Process Engineering. 49:103159. https://doi.org/10.1016/j.jwpe.2022.103159

PUNIA BANGAR S., WHITESIDE W.S., DUNNO K.D., CAVENDER G.A., DAWSON P., LOVE R. (2022) Starch-based bio-nanocomposites films reinforced with cellulosic nanocrystals extracted from Kudzu (Pueraria montana) vine. International Journal Biology and Macromolecular. 203:350–360. https://doi.org/10.1016/j.ijbiomac.2022.01.133

RAHAMAN M.H., ISLAM M.A., ISLAM M.M., RAHMAN M.A., ALAM N.S. (2021) Biodegradable composite adsorbents of modified cellulose and chitosan to remove heavy metal ions from aqueous solution. Current Research Green Sustainaible Chemistry .100119. https://doi.org/10.1016/j.crgsc.2021.100119.

SALCEDO A.F.M., BALLESTEROS F.C., VILANDO A.C., LU M.C. (2016) Nickel recovery from synthetic Watts bath electroplating wastewater by homogeneous fluidized bed granulation process. Separation Purification

DOI: 10.6092/issn.2281-4485/18602

Technology. 169:128–136. https://doi.org/10.1016/j.seppur.2016.06.010.

SHAHNAZ T.S., NARAYANASAMY S. (2020) Surface modification of nanocellulose using polypyrrole for the adsorptive removal of Congo red dye and chromium in binary mixture. International Journal Biology Macromolecular, 151:322–332. https://doi.org/10.1016/j.ijbiomac.2020.02.181.

SHOJAEIARANI J., BAJWA D., SHIRZADIFAR A. (2019) A review on cellulose nanocrystals as promising biocompounds for the synthesis of nanocomposite hydrogels. *Carbohydrade Polymers*. 216:247–259. https://doi.org/10.1016/j.carbpol.2019.04.033.

TANG X., LI Q., WU M., LIN L., SCHOLZ M. (2016) Review of remediation practices regarding cadmium-enriched farmland soil with particular reference to China. Journal Environemental Management 181:646–662. https://doi.org/10.1016/j.jenvman.2016.08.043

VINCENT S., KANDASUBRAMANIAN B. (2021) Cellulose nanocrystals from agricultural resources: Extraction and functionalisation. Europe Polymers Journal 160:11 0789.https://doi.org/10.1016/j.eurpolymj.2021.110789

VISHNU PRIYAN V., KUMAR N., NARAYANASAMY S. (2021) Development of Fe_3O_4/CAC nanocomposite for the effective removal of contaminants of emerging concerns (Ce^{3+}) from water: An ecotoxicological assessment. Environemtal Pollution, 285:117326. https://doi.org/10.1016/j.envpol.2021.117326.

VOISIN H., BERGSTRÖM L., LIU P., MATHEW A.P. (2017) Nanocellulose-Based Materials for Water Purification. https://doi.org/10.3390/nano7030057.

WANG S., YU J., ZHAO P., LI J., HAN S. (2021) Preparation and mechanism investigation of CdS quantum dots applied for copper ion rapid detection. Journal Alloys Compound 854:157195. https://doi.org/10.1016/j.jallcom.2020.157195.

XU H., WANG H., LU Y., ZENG Y., YANG Y., ZHANG Z., WANG H., WANG X., LI L. (2021) CeO_2 quantum dots for highly selective and ultrasensitive fluorescence detection of 4-nitrophenol via the fluorescence resonance energy transfer mechanism. Spectrochimica Acta, Part A: Molecular and Biomolecular Spectroscopy, 262:120115. https://doi.org/10.1016/j.saa.2021.120115.

ZHANG L., ZENG Y., CHENG Z. (2016) Removal of heavy metal ions using chitosan and modified chitosan: A review. Journal Molecular Liquids. 214:175–191. https://doi.org/10.1016/j.molliq.2015.12.013.